Giant, 16, 2023, 100200

Full-length article

# Strength and toughness of tissue adhesives depend on thickness

**Wenlei Zhang [a], Yang Gao [a], Yifan Zhou [a], Hou Wu [a], Zhigang Suo [b,*], Tongqing Lu [a,*]**

[a] State Key Lab for Strength and Vibration of Mechanical Structures, Soft Machines Lab, International Center for Applied Mechanics, Department of Engineering Mechanics, Xi'an Jiaotong University, Xi'an 710049, PR China
[b] John A. Paulson School of Engineering and Applied Sciences, Kavli Institute for Bionano Science and Technology, Harvard University, MA 02138, United States

*Keywords:* Tissue adhesive, Strength, Toughness, Adhesive thickness, Statistical scatter

**Adhesives are commonly assessed by two properties: strength and toughness. Here we study how strength and toughness are affected by adhesive thickness. We sandwich gelatin adhesives of various thicknesses between glass substrates. The transparency of the adhesives and substrates enables us to observe crack nucleation and growth. We measure strength by lap shear of samples without precrack, and measure toughness by lap shear of samples with precrack. Our data show a characteristic adhesive thickness, about 0.5 mm. For adhesives below the characteristic thickness, strength is independent of thickness, but toughness increases with thickness. For adhesives above the characteristic thickness, strength decreases as thickness increases, but toughness is a constant. Strength scatters narrowly for samples of a thin adhesive, but broadly for samples of a thick adhesive. By contrast, toughness scatters narrowly for samples of all thicknesses. This work shows the importance of assessing adhesives of various thicknesses.**

## 1 Introduction

Adhesives for dry and hard materials, such as glasses, ceramics, metals, and plastics, have been used since antiquity [1,2]. Since the mid-20th century, adhesives for wet and soft tissues have been developed for wound closure [3–8], tissue repair [7,9–11], implants [12,13], drug delivery [14,15] and bioelectronics [16–18]. If a tissue adhesive fractures, leakage may cause a second operation, severe complications, and even death. These consequences have been widely reported, including gastrointestinal surgery [19,20], pneumothoracic surgery [21–23], and neurosurgery [24].

Fracture of adhesives are commonly assessed by two properties: strength and toughness. Strength is measured by samples without precrack, and toughness is measured by samples with precrack. Both properties are affected by adhesive thickness [25–29]. In particular, Chai has systematically studied effects of thickness on epoxy adhesives [29–31].

For tissue adhesives, the scatter of strength was reported for twelve commercial products, each of which was subject to three types of tests: tension, lap shear, and peel [32]. For a given tissue adhesive, tensile strength and shear strength often scatter broadly; for example, the tensile strength of the Tissucol fibrin glue ranges over two orders of magnitude. By contrast, peel strength scatters within a factor of 4. Peel strength is measured using samples of precracks, and is interpreted as toughness [33,34].

There has been no systematic report on the effect of thickness on strength and toughness of tissue adhesives. In medical uses, thickness of tissue adhesives commonly ranges from hundreds of micrometers to millimeters. It is important to measure strength and toughness of tissue adhesives of various thicknesses, and report their statistical scatter. Here we measure strength and toughness of a gelatin adhesive of nine thicknesses, ranging from 0.1 mm to 5 mm. For each adhesive thickness, five samples are tested. Tissue adhesives can be assessed by lap shear test (ASTM F2255–05), tension test (ASTM F2256–05) and peel test

* Corresponding authors.
*E-mail addresses:* suo@seas.harvard.edu (Z. Suo), tongqinglu@mail.xjtu.edu.cn (T. Lu).
Received 30 August 2023; Received in revised form 11 October 2023; Accepted 19 October 2023


https://doi.org/10.1016/j.giant.2023.100200

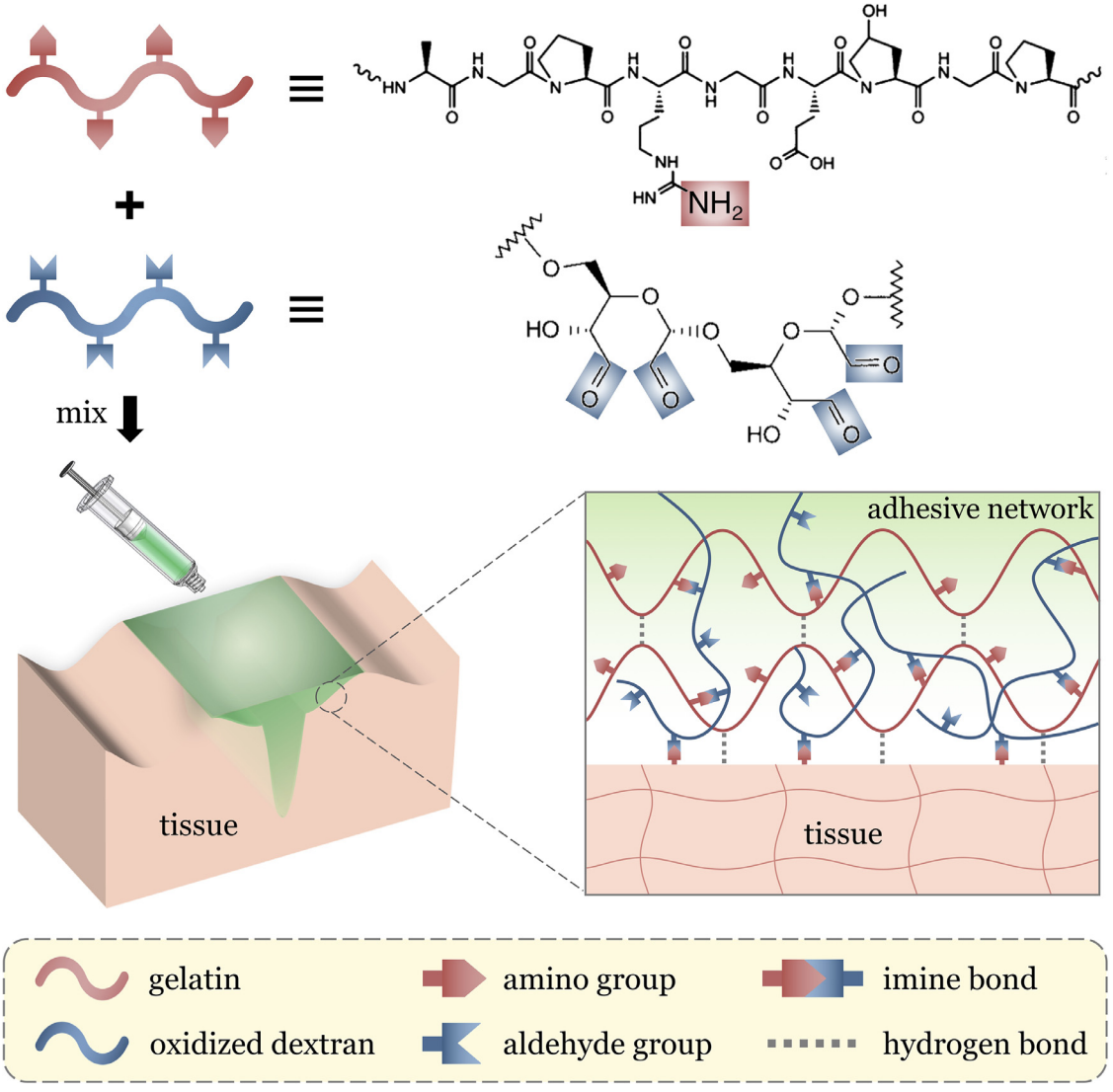


**Fig. 1**

Gelatin tissue adhesive crosslinked by oxidized dextran. The gelatin and tissues contain amino groups (-$NH_2$), and the oxidized dextran contains aldehyde groups (-CHO). An amino group and an aldehyde group condense, resulting in an imine bond (-N=CH-) and a water molecule: R-$NH_2$ + O=CH-R′ = R-N=CH-R′ + $H_2O$. Hydrogen bonds also form between gelatin chains and tissues.

(ASTM F2258). We adopt the lap shear test for its wide use. We measure strength by lap shear without precrack, and measure toughness by lap shear with precrack. We identify a characteristic adhesive thickness, about 0.5 mm. For samples below this characteristic thickness, strength is independent of thickness, but toughness increases with thickness. For samples above the characteristic thickness, strength decreases with thickness, but toughness is independent of thickness. Strength scatters narrowly below the characteristic thickness, but broadly above the characteristic thickness. Toughness scatters narrowly for samples of all thicknesses. This study demonstrates the importance of assessing tissue adhesives of various thicknesses.

## 2 Sample preparation

Gelatin has long been used as adhesives for general applications [35], as well as for medical applications [8]. Here we prepare a gelatin adhesive using oxidized dextran as a crosslinker. Similar systems have been used as tissue adhesives [36,37]. Gelatin and tissues contain amino groups (-$NH_2$) [38], and oxidized dextran contains aldehyde groups (-CHO) [39]. An amino group and an aldehyde group condense, resulting in an imine bond (-N=CH-) and a water molecule: R-$NH_2$ + O=CH-R′ = R-N=CH-R′ + $H_2O$ [39] (Fig. 1). Hydrogen bonds also form between gelatin chains and tissues.

The object of this paper is to study the effect of thickness on tissue adhesives. However, the corrugated surface of tissues may lead to large variation of the measured adhesive properties. Following a common practice in evaluating tissue adhesives, we use rigid and flat glass plates as the adherend in lap shear (ASTM F2255–05). The glass plates are coated with polylysine, which is commonly used to mimic tissues by providing ample amino groups.

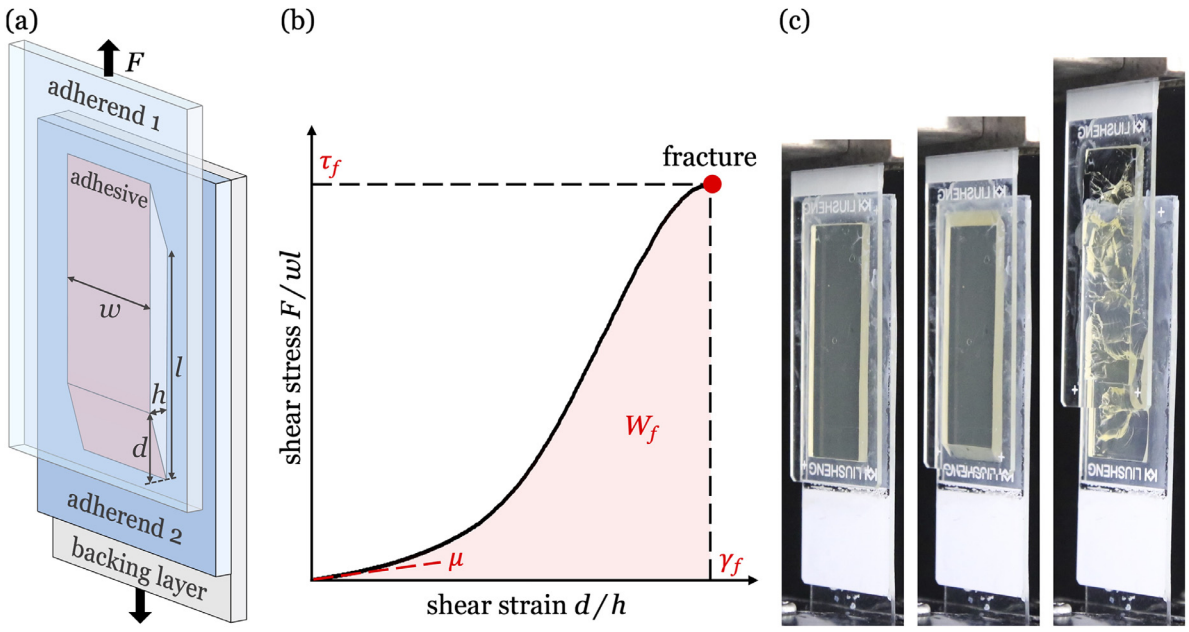


**Fig. 2**

Measure strength by lap shear of samples without precrack. (a) An adhesive is sandwiched between two adherends, which are sheared by a pair of forces. (b) Stress-strain curve. (c) Photos of a sample before, during, and after lap shear.

All chemicals are purchased, including gelatin (from porcine skin, Type A, 300 g Bloom; Sigma-Aldrich, V900863), dextran ($M_w$ = 20,000 g/mol; Aladdin, D104012), sodium periodate ($NaIO_4$; Aladdin, S104091), potassium phosphate monobasic ($KH_2PO_4$; Aladdin, P104075), sodium phosphate dibasic dodecahydrate ($Na_2HPO_4{\cdot}12H_2O$; Aladdin, S112623), sodium chloride (NaCl; Aladdin, C111535), potassium chloride (KCL; Aladdin, P112133). The polylysine coated glass plates are purchased from LIUSHENG® (Nantong, China). The 1 $\mu$m-thick polyethylene glycol terephthalate (PET) single-sided adhesive tape is purchased from XUANNISI Tape (Shanghai, China). The 1 mm-thick PET film is purchased from JINYIHONG Plastics (Dongguan, China)

The oxidized dextran is prepared as follows. We prepare a 10 wt% (solute-to-solution mass ratio) aqueous solution of dextran and then prepare a 10 wt% aqueous solution of $NaIO_4$. We mix the two solutions for a dextran-to-$NaIO_4$ mole ratio of 1:1.5. The mixture is stirred for 12 h in a dark area at room temperature of 25 °C. The resulting solution is transferred into dialysis membrane tubes with the molecular-weight cutoff of 5000 Da and dialyzed in deionized water for 3 days. The deionized water is changed six times daily. The solution is dried by a freeze-drying machine (BIOCOOL FD-1A-80) for three days to sublimate all the water. The powder of oxidized dextran is obtained. The dialdehyde content of the oxidized dextran is measured at the average of 92.92 % by an existing method [40].

The phosphate buffered saline (PBS) is prepared as follows. We prepare 0.2 mol/L $Na_2HPO_4$ solution and 0.2 mol/L $KH_2PO_4$ solution. For 100 g of PBS solution, we mix 81 g of $Na_2HPO_4$ solution with 19 g of $KH_2PO_4$ solution and then add 0.8 g of NaCl and 0.02 g of KCL. The final PBS has a pH of 7.3, measured by a pH meter (Sartorius PB-10). The PBS solution is used as the solvent of the precursor of tissue adhesives.

The samples without precrack are prepared as follows. We dissolve gelatin into PBS to prepare a solution of 20 wt% gelatin. The solution is sealed and stirred at 37 °C for 30 min to fully dissolve gelatin. We dissolve the previously prepared oxidized dextran into PBS to prepare a solution of 20 wt% dextran. The solution is sealed and stirred at 37 °C for 10 min. The gelatin solution is drawn into one syringe, and the dextran solution is drawn into another syringe. The mass ratio of the gelatin solution to the dextran solution in the syringes is fixed at 100:1. The two syringes are connected by a joint and pushed back and forth to mix the two solutions. We immediately inject the mixture into a silicone rubber spacer sandwiched by two polylysine coated glass plates. The samples are sealed and cured at 37 °C for 1 h in an oven (Bluepard BPG-9140A). The prepared samples without precrack have the length $l = 45$mm, width $w = 15$mm, and thickness $h$ ranging from 0.1 mm to 5 mm (Fig. 2a).

The samples with precrack are prepared as follows. A 1 $\mu$m-thick PET single-sided adhesive tape is applied on one glass plate. The other side of PET tape does not adhere to the tissue adhesive. The tissue adhesive is applied between the two glass plates. The curing procedure is the same as the preparation of the samples without precrack. The prepared samples with precrack have the crack length $c = 15$mm and bonding length $l = 30$mm (Fig. 8a).

To maintain water content, the as-prepared samples are stored in a sealed polyethylene bag before the tests.

## 3 Strength

We measure strength by lap shear of samples without precrack (Fig. 2a). The samples are clamped by the grippers of a tensile tester (SHIMADZU AGS-X) with a load cell of 1 kN. When the samples

are thin, the direct clamping of samples may cause bending of glass plates, which introduces a large error to the measurement of force. In this work, we glue one glass plate of the samples on a backing layer of 1 mm-thick PET film. The backing layer is flexible but inextensible. The sample is sheared by a pair of forces $F$ and the two glass plates shear by displacement $d$. The strain rate, defined as the displacement rate divided by the adhesive thickness, is fixed at 10/min for all samples. The tensile tester applies a monotonic load to each sample until the sample fractures. The force-displacement curve is recorded by the tensile tester. The fracture process is recorded by a digital camera (Canon EOS5D). The test is carried out at the room temperature of 25 °C in the open air. The duration of each test is less than 2 min, so that the water content of the tissue adhesive remains almost unchanged during the test.

A representative stress-strain curve of a sample without precrack is shown in Fig. 2(b). The shear stress is defined as the force divided by the bonding area, $F/wl$. The shear strain is defined as the displacement divided by the adhesive thickness, $d/h$. The stress and strain at fracture define the strength $\tau_f$ and the fracture strain $\gamma_f$. We calculate the shear modulus by the linear fit of the stress-strain curve for the first 10 % of strain, and the work of fracture $W_f$ by integrating the area under the stress-strain curve. All the samples fracture cohesively (Fig. 2c).

We measure stress-strain curves using samples of nine adhesive thicknesses (0.1 mm, 0.2 mm, 0.3 mm, 0.5 mm, 0.8 mm, 1 mm, 2 mm, 3 mm, 5 mm) (Fig. 3). For each thickness, five samples are tested. Note that strength has a narrow scatter among samples of thinner adhesive (Fig. 3a-3d), but has a wide scatter among samples of thicker adhesive (Fig. 3e-3i). The samples of thinner adhesive have higher strength and fracture strain than those of thicker adhesive (Fig. 3j). By contrast, the shear modulus of all the samples are similar and show a narrow scatter.

We plot the shear modulus $\mu$, strength $\tau_f$, fracture strain $\gamma_f$, and work of fracture $W_f$ as functions of adhesive thickness $h$ (Fig. 4). The shear modulus is almost independent of adhesive thickness and has a mean value of 8.28 kPa. The strength is independent of thickness with the mean value of 296 kPa when $h < 0.5$mm, and decreases with thickness when $h > 0.5$mm. The fracture strain and work of fracture decreases as thickness increases.

To evaluate the statistical variation from sample to sample, we use the coefficient of variation (CV), defined by the standard deviation divided by the mean. We plot the CV of the measured shear modulus $\mu$, strength $\tau_f$, fracture strain $\gamma_f$ and work of fracture $W_f$ at each adhesive thickness $h$ (Fig. 5). The modulus is set by the average behavior of the polymer network, and has narrow statistical variation from sample to sample. Thus, we use the CV of shear modulus, about 0.1, as a reference value. We find that the strength and work of fracture show a similar narrow scatter as shear modulus when $h < 0.5$mm, but scatter more broadly than shear modulus when $h > 0.5$mm. The scatter of fracture strain in the whole thickness range is comparable to the scatter of shear modulus.

The statistical scatter of strength originates from different kinds of stress concentrators in the sample. First, a sample inevitably contains interior flaws and edge flaws, such as gas bubbles (Fig. 6a, b). Second, in fabricating a sample, the layer of adhesive does not cover the entire area of each adherend. Each edge of the adhesive intersects with the adherend and forms a corner. The shape of the corner is uncontrolled, and varies from sample to sample (Fig. 6c, d).

A corner with a small radius of curvature concentrates stress more than a corner of a large radius of curvature. These stress concentrators knock down the measured strength. As the flaw size is random, the strength scatters. The thicker the adhesive, the more probable of large flaws, and the lower the strength. For example, the largest edge bubble is 1.9 mm in diameter in the samples with a thickness of 5 mm, and is 0.2 mm in the samples with a thickness of 0.3 mm. The effect of corners on strength of a polyacrylamide hydrogel under lap shear has been studied recently [41], which shows that the strength also decreases as the thickness increases. However, the polyacrylamide used in that study is brittle and highly elastic. It is unclear that the interpretation proposed in that paper applies to our data here.

The transparency of the glass plates and the adhesive enables us to observe the nucleation and growth of cracks. We videotape each sample during lap shear. The configuration of samples is shown in Fig. 2(a) and the camera is placed in front of the samples. Cracks can nucleate from interior flaws (Fig. 7a), side edges (Fig. 7b), and the front edges (Fig. 7c, d). The sites of crack nucleation seem to be random, and do not correlate with adhesive thickness (Fig. 7e). In some samples, cracks first grow like tunnels, and then the tunnels merge, leading to fracture (Fig. 7a, b, c, Movie 1). In other samples, cracks do not grow like tunnels, but grow along fronts (Fig. 7d, Movie 2). Thin adhesives are more likely to grow by tunnels, but thick adhesives are more likely to grow by fronts (Fig. 7f).

## 4 Toughness

We measure toughness by lap shear of samples with precrack (Fig. 8a). We introduce a precrack by adhering a 1 $\mu$m-thick PET tape on one glass plate of the samples. The other side of PET tape does not adhere to the adhesives. The length of the PET tape, and therefore the length of crack, is 15 mm, much larger than the thickness of the adhesive. The as-prepared samples with a precrack are monotonically loaded by the tensile tester until fracture. The loading procedure is the same as that of the samples without precrack.

For a sample with a precrack of length much larger than the adhesive thickness, when one rigid adherend shears relative to the other, the energy release rate takes the form [28]:

$$G = hW(\lambda) \tag{1}$$

where $W(\lambda)$ is the strain energy per unit volume of the adhesive under a homogeneous shear strain $\gamma$.

The precrack does not grow when the shear strain $\gamma$ is small, and grows when the shear strain reaches a critical value $\gamma_C$. The critical energy release rate, $G_C$, defines toughness:

$$G_C = hW(\gamma_C) \tag{2}$$

A representative stress-strain curve of a sample with precrack is shown in Fig. 8(b). As the region of inhomogeneous deformation around the crack front is much smaller than the region of homogeneous deformation, the normalized force-displacement curve of the precracked sample before fracture is

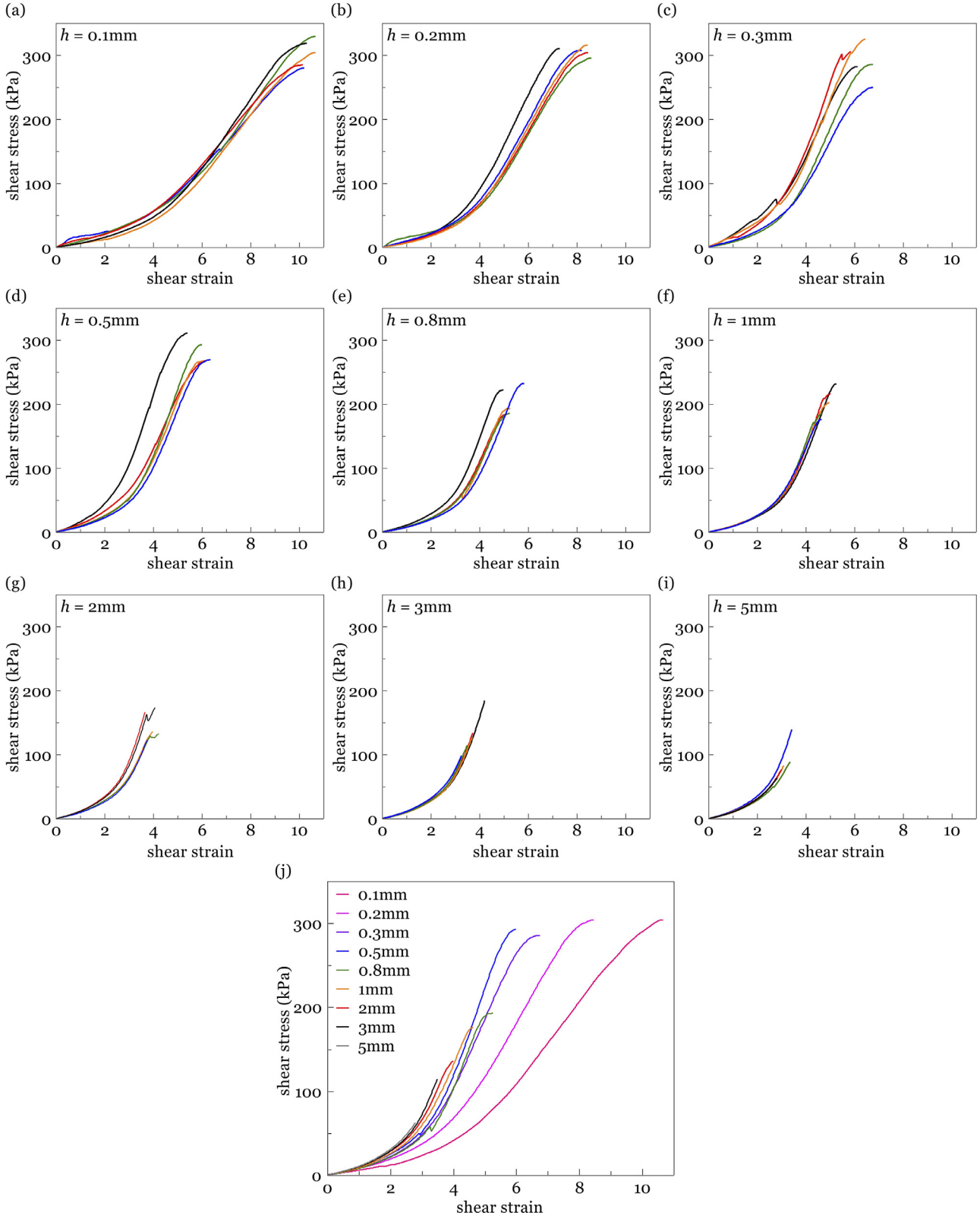


**Fig. 3**

The stress-strain curves of the samples without precrack at nine adhesive thicknesses *h*. (a)-(i) For each adhesive thickness, five samples are tested. (j) Nine representative curves for each adhesive thickness for better comparison.

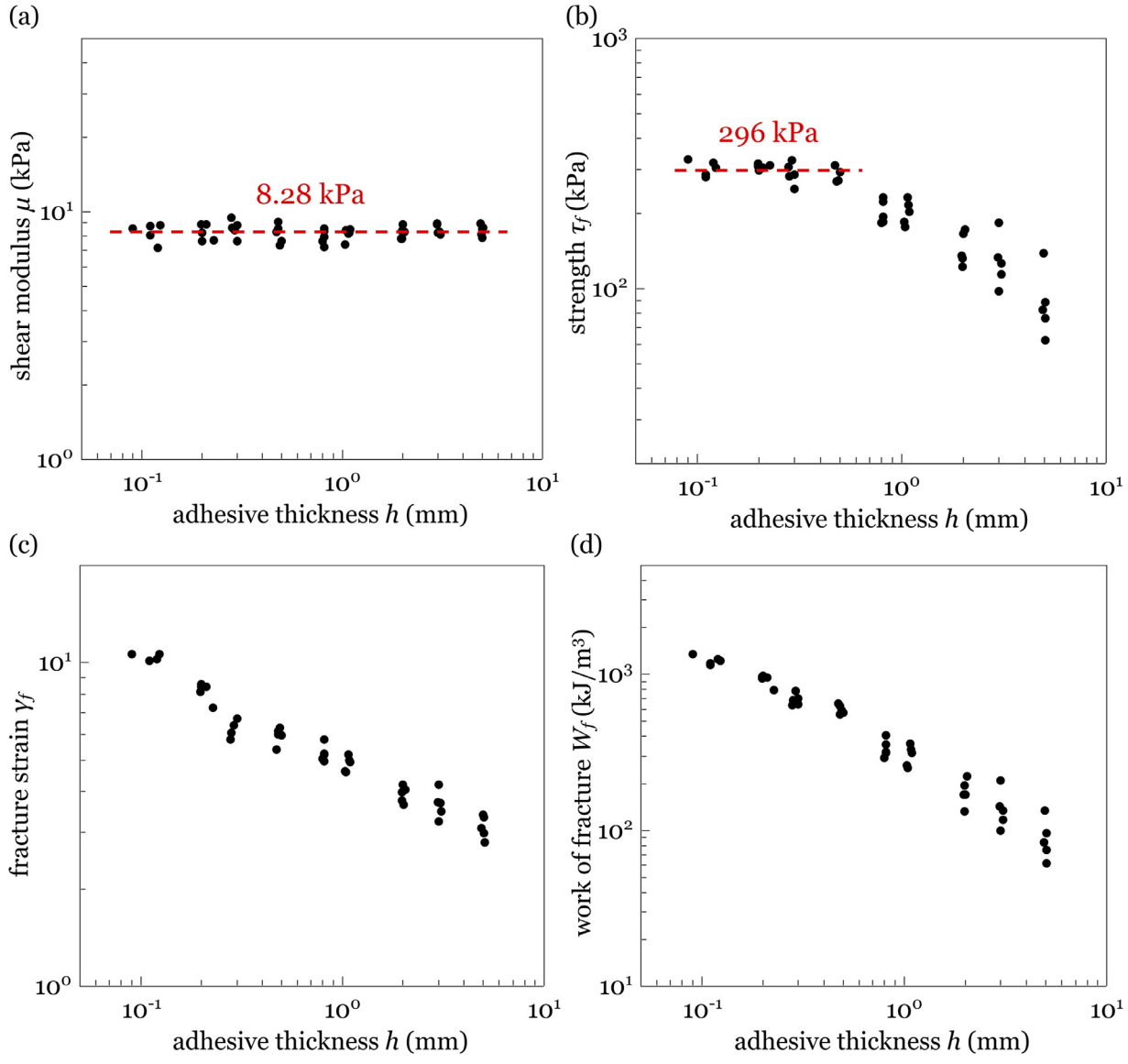


**Fig. 4**

The measured shear modulus $\mu$, strength $\tau_f$, fracture strain $\gamma_f$, and work of fracture $W_f$ as functions of adhesive thickness $h$.

approximately the same as the adhesive under homogeneous shear. Consequently, $W(\gamma_C)$ can be calculated by integrating the area under the stress-strain curve of the precracked samples to the critical strain $\gamma_C$. All the samples with precrack also fracture cohesively in the bonding region (Fig. 8c).

We measure the stress-strain curves using the precracked samples of nine adhesive thicknesses (Fig. 9). For each thickness, five samples are tested. Examine the stress-strain curve of every sample, we note the following common features. When the strain is small, the PET film remains bonded to the adhesive, and the stress-strain curve is smooth. When the strain reaches some value, the PET film detaches from the adhesive, and the stress drops somewhat suddenly. As the strain increases further, the crack front at the edge of the PET film does not grow, and the stress-strain curve becomes smooth again. When the strain reaches a critical value, the crack advances, and the sample soon fractures. Note that the strength and critical strain of the precracked samples of all adhesive thicknesses show narrow scatters (Fig. 9a-9i). The samples of thinner adhesive have higher strength and critical strain than those of thicker adhesive (Fig. 9j).

We plot the toughness $G_C$ and the coefficient of variation (CV) as functions of adhesive thickness $h$ (Fig. 10). The mean value of toughness increases with thickness when $h < 0.5$mm, and reaches a plateau at 247 J/m$^2$ when $h > 0.5$mm. The CV of toughness over the whole thickness range is between 0.03 and 0.13, comparable to that of shear modulus.

We videotape the experiment of every sample, and observe the nucleation and growth of the crack. Fig. 11(a) shows a sharp precrack tip introduced by adhering a 1 $\mu$m-thick PET tape on one adherend. The radius of the precrack tip is set by the thickness of PET tape. As the precrack is sharp enough to concentrate stress, cracks always nucleate from the precrack tip. Therefore,

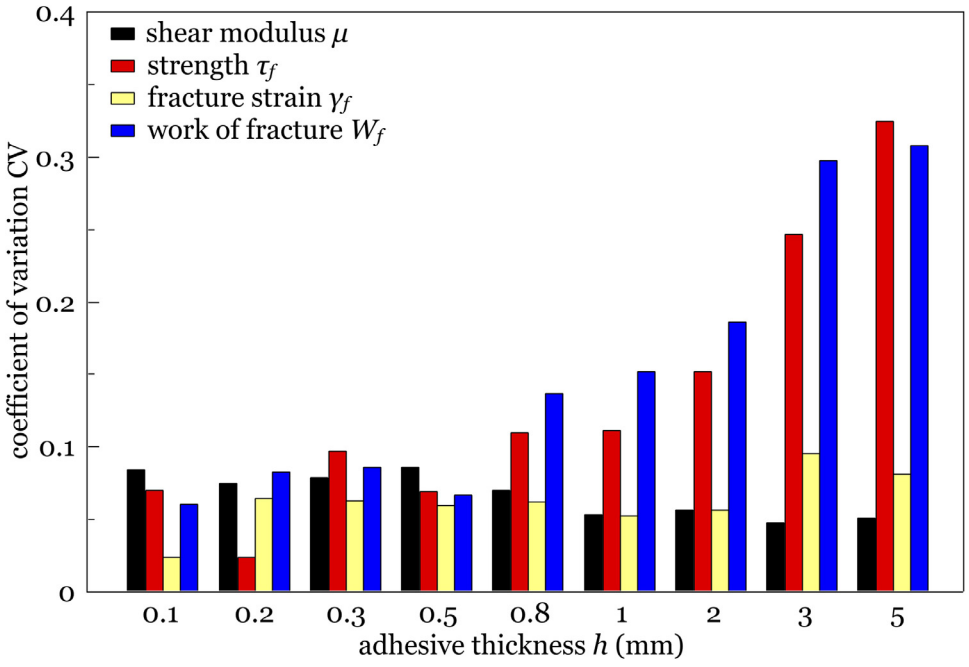


**Fig. 5**

Coefficient of variation (CV) of shear modulus $\mu$, strength $\tau_f$, fracture strain $\gamma_f$, and work of fracture $W_f$ for samples of each adhesive thickness $h$.

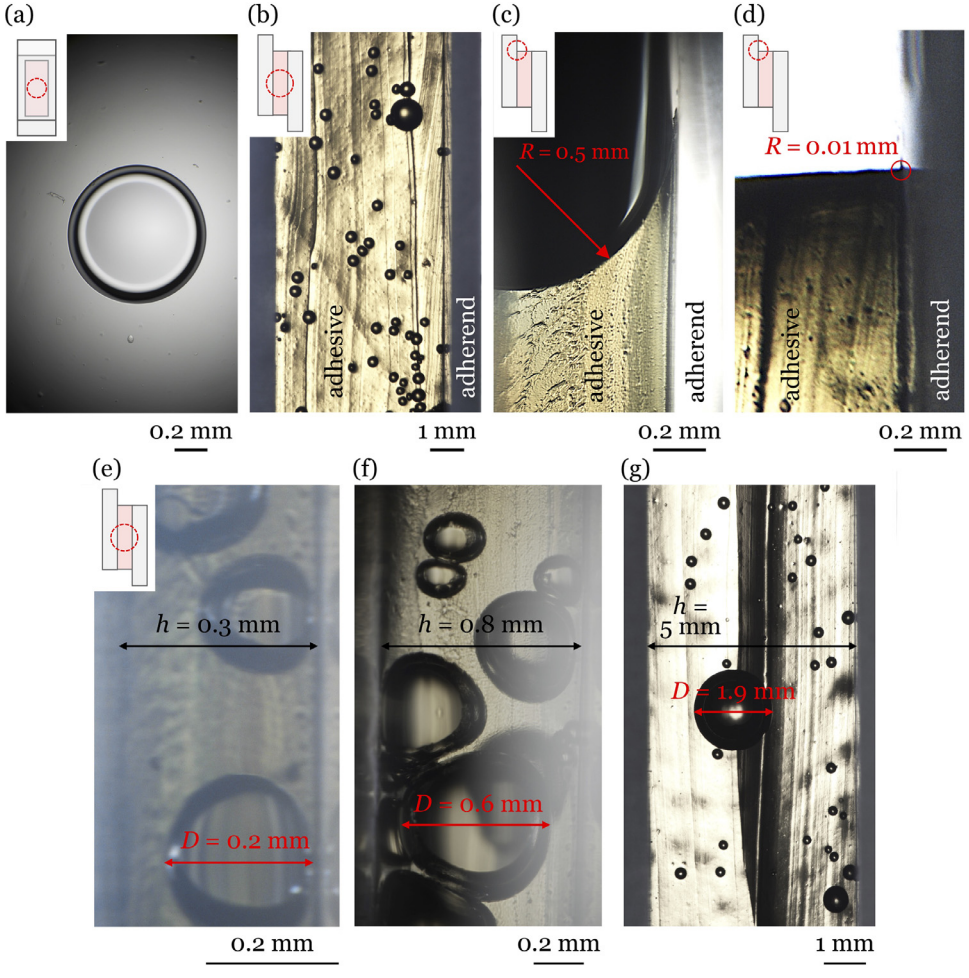


**Fig. 6**

Cracks nucleate from stress concentrators. (a) Interior flaws. (b) Edge flaws. (c) A corner with a large radius of curvature. (d) A corner with a small radius of curvature.

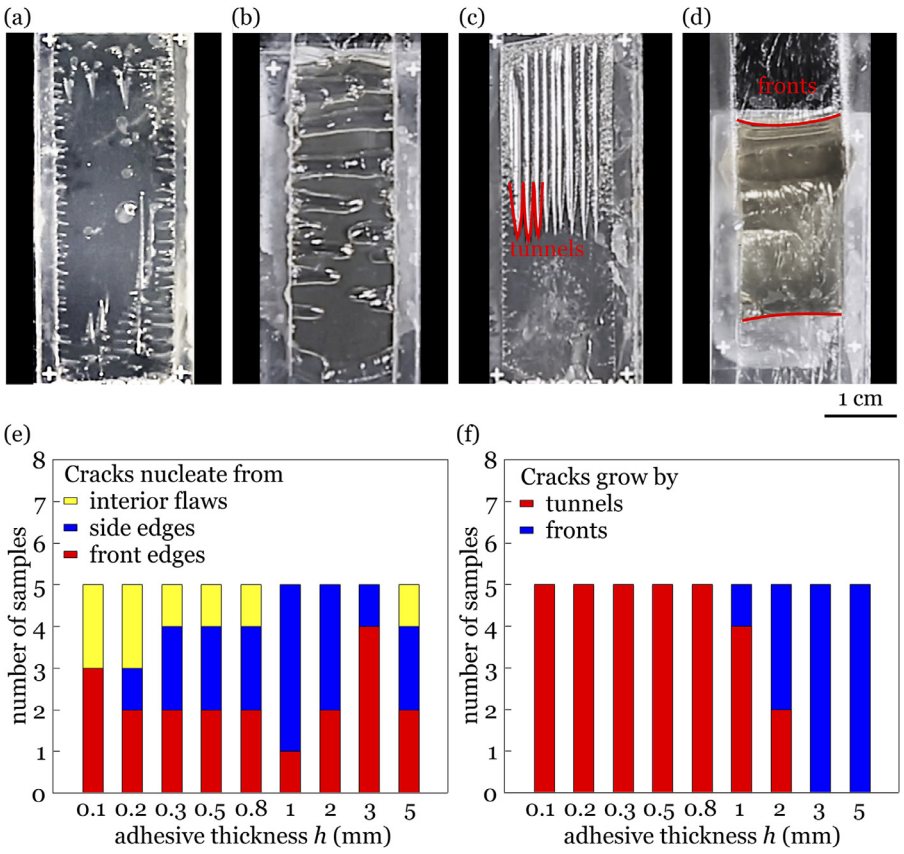


**Fig. 7**

For samples without precrack, cracks nucleate from (a) interior flaws, (b) side edges, and (c, d) front edges. In some samples, cracks grow like tunnels. In other samples, cracks grow along fronts. (e) The observed sites of crack nucleation of 45 samples. (f) The observed types of crack growth of 45 samples.

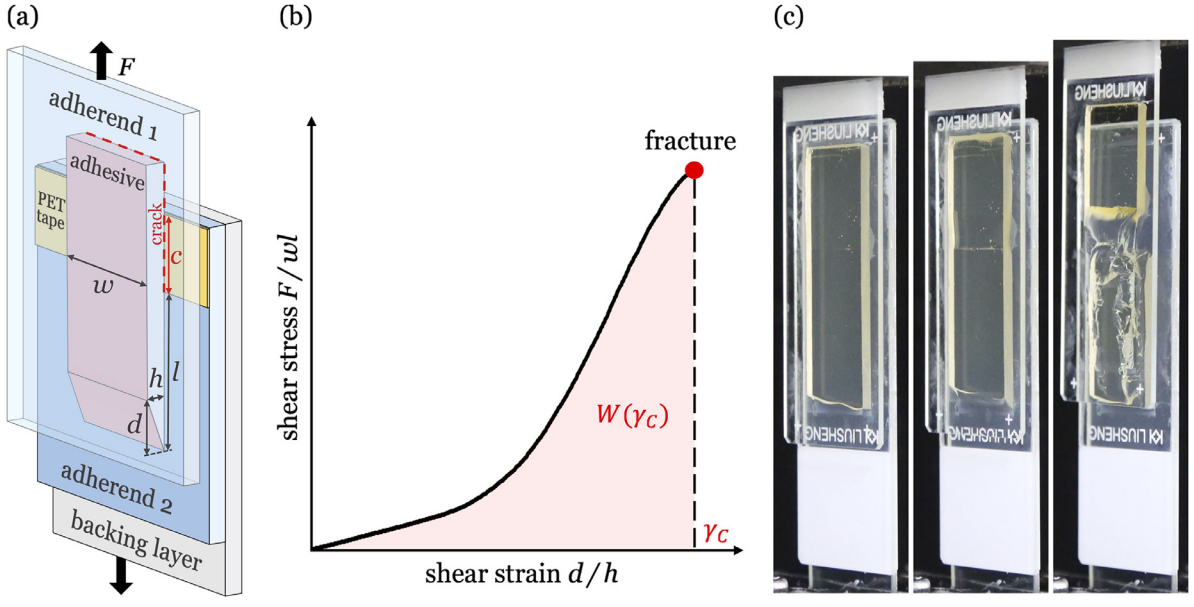


**Fig. 8**

Measure toughness by lap shear of samples with precrack. (a) A sample with a precrack, length *c*, is sheared by a pair of forces. (b) Stress-strain curve. (c) Photos of a sample before, during, and after lap shear.

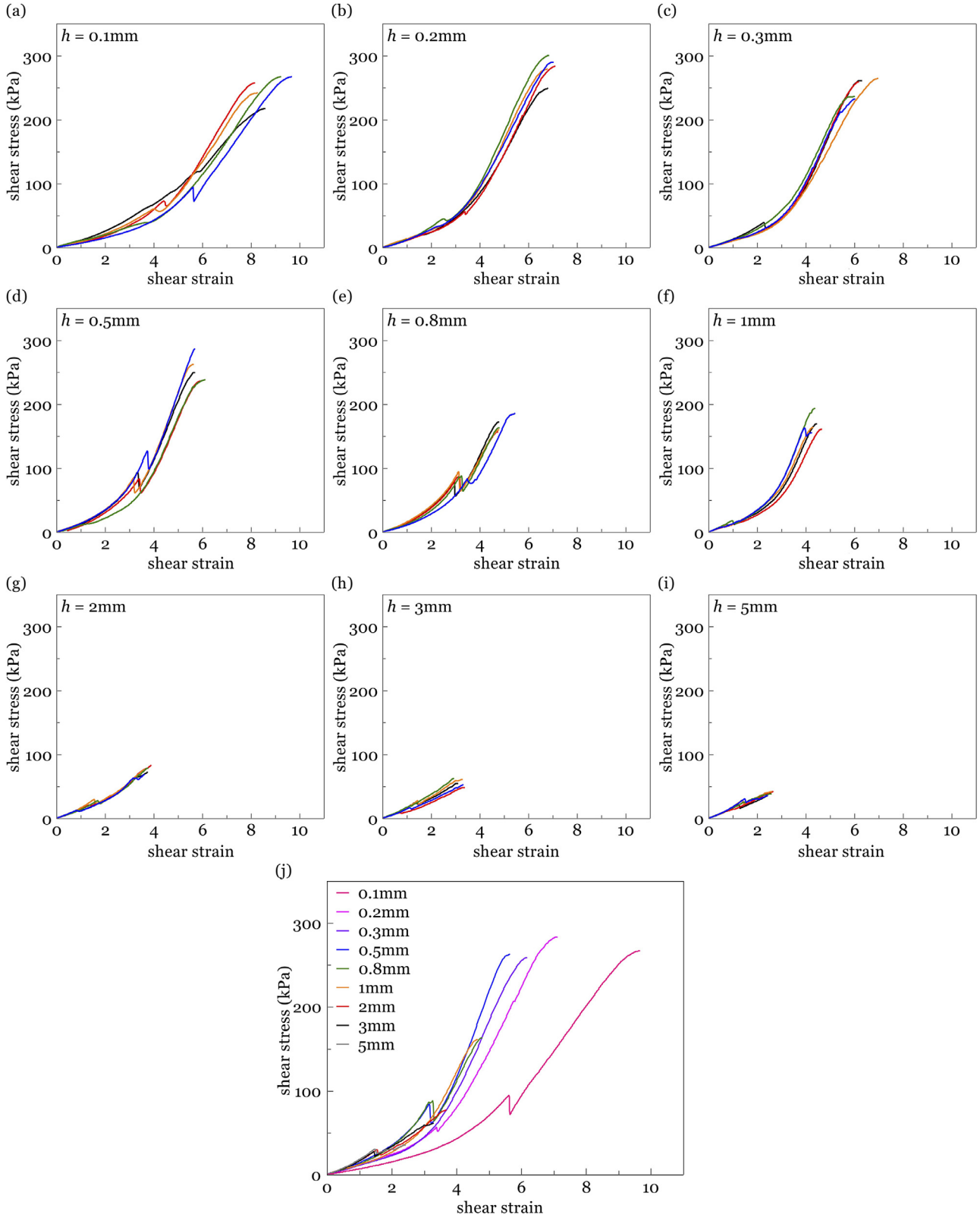


**Fig. 9**

The stress-strain curves of the samples with precrack at nine adhesive thicknesses *h*. (a)-(i) For each adhesive thickness, five samples are tested. (j) Nine representative curves for each adhesive thickness for better comparison.

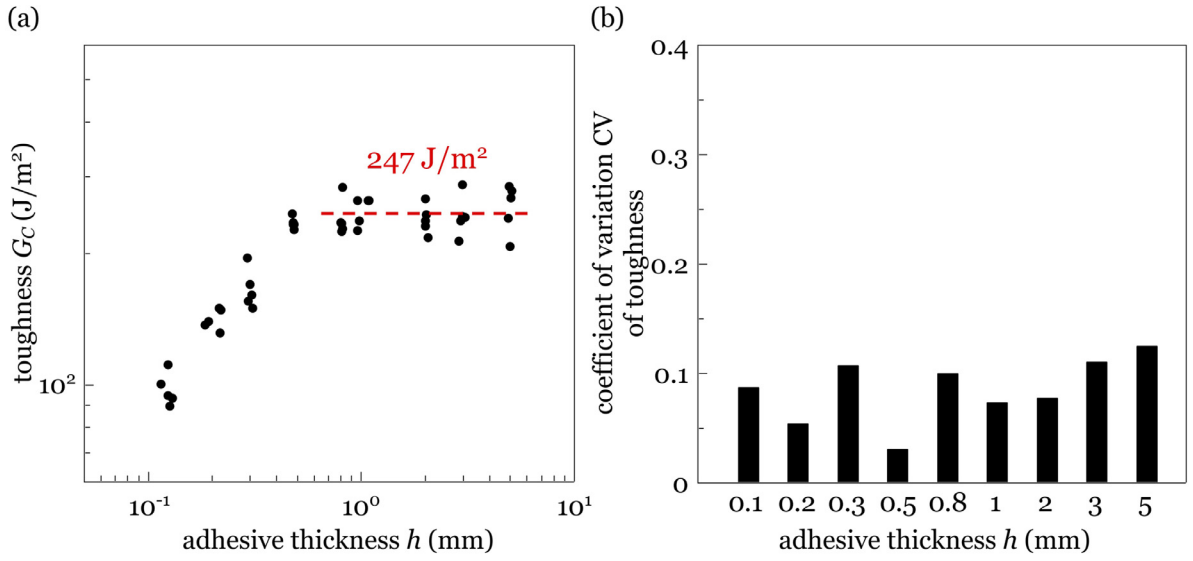


**Fig. 10**

(a) Toughness $G_C$ as a function of adhesive thickness $h$. (b) The coefficient of variation CV of toughness for samples of each adhesive thickness $h$.

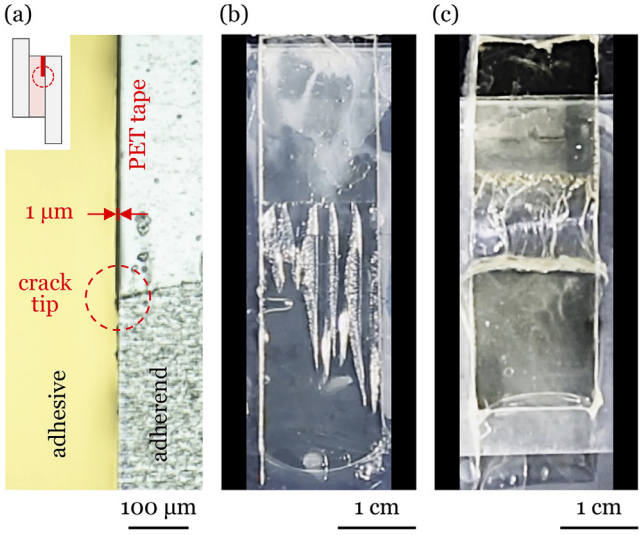


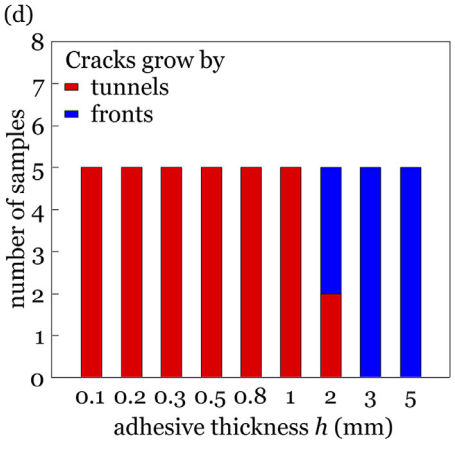


**Fig. 11**

For samples with precrack, cracks nucleate from a precrack. (a) A precrack introduced by adhering a 1 um-thick PET tape on one adherend of the sample. Cracks grow from the precrack tip (b) by tunnels, or (c) by fronts. (d) The observed types of crack growth of 45 samples.

the stress-strain curves of samples with precrack scatter narrowly for all adhesive thicknesses. In some samples, cracks grow by tunnels (Fig. 11b, Movie 3). In other samples, cracks grow by fronts (Fig. 11c, Movie 3). Thin adhesives tend to grow by tunnels, but thick adhesives tend to grow by fronts (Fig. 11d).

The thickness dependence of toughness can be interpreted using the theory presented in Refs [34,42,43]. For thin adhesives, the fracture process zone is comparable to the adhesive thickness, and toughness is linear in adhesive thickness. For thick adhesives, the fracture process zone is smaller than the adhesive thickness, and toughness is independent of adhesive thickness.

## 5 Discussion

Despite of the extensive studies on the thickness dependence of adhesives such as epoxy and hydrogel [28–31], this paper focuses on the thickness dependence of tissue adhesive. Whereas tissue adhesives have long been used in medical applications [8,35], the existing methods of evaluating strength of tissue adhesives are still immature. This paper demonstrates that below the characteristic thickness, strength is independent of thickness and can be regarded as a material parameter to evaluate the tissue adhesives. However, in most cases, the thickness used in medical applications is often above the characteristic thickness [44], where toughness should be taken as the evaluation index for the tissue adhesive. These findings may help to establish a standard to evaluate mechanical properties of tissue adhesives. We also highlight that the use of transparent adherends in our experiment enables direct observations of fracture process at the adhesive interface. Various of fracture modes have been observed (Figs. 7, 11). Notably, these complex fracture phenomena as well as the highly nonlinear nature of the adhesive material impose a great challenge to establish a simple mechanics model to predict the characteristic thickness, which deserves further studies.

## 6 Conclusions

We have studied how adhesive thickness affects strength and toughness. We sandwich a gelatin adhesive between two glass substrates. We measure strength by lap shear of samples without precrack, and measure toughness by lap shear of samples with precrack. The transparency of the glass substrates and the adhesive enables us to observe crack nucleation and growth. For a sample without precrack, cracks can nucleate from internal flaws, side edges, or front edges. For a sample prepared with a thin PET film between a glass substrate and the adhesive, cracks always nucleate from the edge of the PET film. In both cases, cracks can grow by either tunnels or fronts. Our data show a characteristic adhesive thickness, about 0.5 mm. For adhesives below the characteristic thickness, strength is independent of thickness, but toughness increases with thickness. For adhesives above the characteristic thickness, strength decreases as thickness increases, but toughness is a constant. Strength scatters narrowly for samples of a thin adhesive, but broadly for samples of a thick adhesive. By contrast, toughness scatters narrowly for samples of all thicknesses. This work indicates that both strength and toughness of an adhesive should be measured as functions of thickness.

## Declaration of Competing Interest

There are no conflicts of interest to declare.

## Data availability

Data will be made available on request.

## CRediT authorship contribution statement

**Wenlei Zhang:** Conceptualization, Methodology, Formal analysis, Investigation, Visualization, Writing – original draft. **Yang Gao:** Methodology. **Yifan Zhou:** Methodology. **Hou Wu:** Methodology. **Zhigang Suo:** Conceptualization, Writing – review & editing, Supervision, Project administration. **Tongqing Lu:** Conceptualization, Resources, Writing – review & editing, Supervision, Project administration.

## Acknowledgments

YG acknowledges the support of NSFC, China (12172274).

## Supplementary materials

Supplementary material associated with this article can be found, in the online version, at doi:10.1016/j.giant.2023.100200.

### References


[1] S. Ebnesajjad, A.H. Landrock, Adhesives Technology Handbook, William Andrew, Norwich, 2014.

[2] A.J. Kinloch, Adhesion and adhesives: Science and Technology, Springer Science & Business Media, New York, 2012.

[3] R. Jain, S. Wairkar, Recent developments and clinical applications of surgical glues: an overview, Int. J. Biol. Macromol. 137 (2019) 95–106, doi:10.1016/j.ijbiomac.2019.06.208.

[4] Y. Gao, X. Han, J. Chen, Y. Pan, M. Yang, L. Lu, J. Yang, Z. Suo, T. Lu, Hydrogel-mesh composite for wound closure, Proc. Natl. Acad. Sci. U. S. A. 118 (2021) e2103457118, doi:10.1073/pnas.2103457118.

[5] K. Liu, H. Yang, G. Huang, A. Shi, Q. Lu, S. Wang, W. Qiao, H. Wang, M. Ke, H. Ding, T. Li, Y. Zhang, J. Yu, B. Ren, R. Wang, K. Wang, H. Feng, Z. Suo, J. Tang, Y. Lv, Adhesive anastomosis for organ transplantation, Bioact. Mater. 13 (2022) 260–268, doi:10.1016/j.bioactmat.2021.11.003.

[6] N. Annabi, Y.N. Zhang, A. Assmann, E.S. Sani, G. Cheng, A.D. Lassaletta, A. Vegh, B. Dehghani, G.U. Ruiz-Esparza, X. Wang, S. Gangadharan, A.S. Weiss, A. Khademhosseini, Engineering a highly elastic human protein-based sealant for surgical applications, Sci. Transl. Med. 9 (2017) eaai7466, doi:10.1126/scitranslmed.aai7466.

[7] J. Li, A.D. Celiz, J. Yang, Q. Yang, I. Wamala, W. Whyte, B.R. Seo, N.V. Vasilyev, J.J. Vlassak, Z. Suo, D.J. Mooney, Tough adhesives for diverse wet surfaces, Science 357 (2017) 378–381, doi:10.1126/science.aah6362.

[8] G.M. Taboada, K. Yang, M.J.N. Pereira, S.S. Liu, Y. Hu, J.M. Karp, N. Artzi, Y. Lee, Overcoming the translational barriers of tissue adhesives, Nat. Rev. Mater. 5 (2020) 310–329, doi:10.1038/s41578-019-0171-7.

[9] B. Sharma, S. Fermanian, M. Gibson, S. Unterman, D.A. Herzka, B. Cascio, J. Coburn, A.Y. Hui, N. Marcus, G.E. Gold, J.H. Elisseeff, Human cartilage repair with a photoreactive adhesive-hydrogel composite, Sci. Transl. Med. 5 (2013) 167ra6, doi:10.1126/scitranslmed.3004838.

[10] N. Lang, M.J. Pereira, Y. Lee, I. Friehs, N.V. Vasilyev, E.N. Feins, K. Ablasser, E.D. O'Cearbhaill, C. Xu, A. Fabozzo, R. Padera, S. Wasserman, F. Freudenthal, L.S. Ferreira, R. Langer, J.M. Karp, P.J. Del Nido, A blood-resistant surgical glue for minimally invasive repair of vessels and heart defects, Sci. Transl. Med. 6 (2014) 218ra6, doi:10.1126/scitranslmed.3006557.

[11] D.A. Wang, S. Varghese, B. Sharma, I. Strehin, S. Fermanian, J. Gorham, D.H. Fairbrother, B. Cascio, J.H. Elisseeff, Multifunctional chondroitin sulphate for cartilage tissue-biomaterial integration, Nat. Mater. 6 (2007) 385–392, doi:10.1038/nmat1890.

[12] R.J. LaPorte, Hydrophilic Polymer Coatings For Medical Devices, CRC Press, New York, 2017.

[13] H. Cheng, K. Yue, M. Kazemzadeh-Narbat, Y. Liu, A. Khalilpour, B. Li, Y.S. Zhang, N. Annabi, A. Khademhosseini, Mussel-inspired multifunctional hydrogel coating for prevention of infections and enhanced osteogenesis, ACS Appl. Mater. Interfaces. 9 (2017) 11428–11439, doi:10.1021/acsami.6b16779.

[14] J. Li, D.J. Mooney, Designing hydrogels for controlled drug delivery, Nat. Rev. Mater. 1 (2016) 16071, doi:10.1038/natrevmats.2016.71.

[15] T.R. Hoare, D.S. Kohane, Hydrogels in drug delivery: progress and challenges, Polymer (Guildf) 49 (2008) 1993–2007, doi:10.1016/j.polymer.2008.01.027.

[16] C. Yang, Z. Suo, Hydrogel ionotronics, Nat. Rev. Mater. 3 (2018) 125–142, doi:10.1038/s41578-018-0018-7.

[17] H. Yuk, B. Lu, X. Zhao, Hydrogel bioelectronics, Chem. Soc. Rev. 48 (2019) 1642–1667, doi:10.1039/c8cs00595h.

[18] H.R. Lee, C.C. Kim, J.Y. Sun, Stretchable ionics – A promising candidate for upcoming wearable devices, Adv. Mater. 30 (2018) 1704403, doi:10.1002/adma.201704403.

[19] T. Nordentoft, Sealing of gastrointestinal anastomoses with fibrin glue coated collagen patch, Dan. Med. J. 62 (2015) B5081.

[20] J.A. Sapala, M.H. Wood, M.P. Schuhknecht, Anastomotic leak prophylaxis using a vapor-heated fibrin sealant: report on 738 gastric bypass patients, Obes. Surg. 14 (2004) 35–42, doi:10.1381/096089204772787266.

[21] C. Tan, M. Utley, C. Paschalides, J. Pilling, J.D. Robb, K.M. Harrison-Phipps, L. Lang-Lazdunski, T. Treasure, A prospective randomized controlled study to assess the effectiveness of CoSeal® to seal air leaks in lung surgery, Eur. J. Cardio-Thoracic Surg. 40 (2011) 304–308, doi:10.1016/j.ejcts.2010.11.079.

[22] H. Miyamoto, T. Futagawa, Z. Wang, A. Yamazaki, A. Morio, S. Sonobe, H. Izumi, Y. Hosoda, E. Hata, Fibrin glue and bioabsorbable felt patch for intraoperative intractable air leaks, Japanese J. Thorac. Cardiovasc. Surg. 51 (2003) 232–236, doi:10.1007/s11748-003-0019-2.

[23] J. Passage, R. Tam, M. Windsor, M. O'Brien, Bioglue: a review of the use of this new surgical adhesive in thoracic surgery, ANZ J. Surg. 75 (2005) 315–318, doi:10.1111/j.1445-2197.2005.03350.x.

[24] K.H. Siedentop, K. O'Grady, J.J. Park, T. Bhattacharya, B. Sanchez, Fibrin sealant for treatment of cerebrospinal fluid leaks, Am. J. Otol. 20 (1999) 777–780.

[25] L.F.M. da Silva, T.N.S.S. Rodrigues, M.A.V. Figueiredo, M.F.S.F. de Moura, J.A.G. Chousal, Effect of adhesive type and thickness on the lap shear strength, J. Adhes. 82 (2006) 1091–1115, doi:10.1080/00218460600948511.

[26] L.D.R. Grant, R.D. Adams, L.F.M. da Silva, Experimental and numerical analysis of single-lap joints for the automotive industry, Int. J. Adhes. Adhes. 29 (2009) 405–413, doi:10.1016/j.ijadhadh.2008.09.001.

[27] A.A. Taib, R. Boukhili, S. Achiou, S. Gordon, H. Boukehili, Bonded joints with composite adherends. Part I. Effect of specimen configuration, adhesive thickness, spew fillet and adherend stiffness on fracture, Int. J. Adhes. Adhes. 26 (2006) 226–236, doi:10.1016/j.ijadhadh.2005.03.015.

[28] Y. Wang, X. Yang, G. Nian, Z. Suo, Strength and toughness of adhesion of soft materials measured in lap shear, J. Mech. Phys. Solids. 143 (2020) 103988, doi:10.1016/j.jmps.2020.103988.

[29] H. Chai, Observation of deformation and damage at the tip of cracks in adhesive bonds loaded in shear and assessment of a criterion for fracture, Int. J. Fract. 60 (1993) 311–326, doi:10.1007/BF00034739.

[30] H. Chai, Deformation and failure of adhesive bonds under shear loading, J. Mater. Sci. 28 (1993) 4944–4956, doi:10.1007/BF00361160.

[31] H. Chai, The effects of bond thickness, rate and temperature on the deformation and fracture of structural adhesives under shear loading, Int. J. Fract. 130 (2004) 497–515, doi:10.1023/B:FRAC.0000049504.51847.2a.

[32] K.A. Vakalopoulos, Z. Wu, L. Kroese, G.J. Kleinrensink, J. Jeekel, R. Vendamme, D. Dodou, J.F. Lange, Mechanical strength and rheological properties of tissue adhesives with regard to colorectal anastomosis an ex vivo study, Ann. Surg. 261 (2015) 323–331, doi:10.1097/SLA.0000000000000599.

[33] A.N. Gent, Fracture mechanics of adhesive bonds, Rubber Chem. Technol. 47 (1974) 202–212, doi:10.5254/1.3540427.

[34] A.N. Gent, G.R. Hamed, Peel mechanics of adhesive joints, Polym. Eng. Sci. 17 (1977) 462–466, doi:10.1002/pen.760170708.

[35] L. Skeist, Handbook of Adhesives, Champman & Hall, New York, 1990.

[36] X. Mo, H. Iwata, S. Matsuda, Y. Ikada, Soft tissue adhesive composed of modified gelatin and polysaccharides, J. Biomater. Sci. Polym. Ed. 11 (2000) 341–351, doi:10.1163/156856200743742.

[37] T. Wang, J. Nie, D. Yang, Dextran and gelatin based photocrosslinkable tissue adhesive, Carbohydr. Polym. 90 (2012) 1428–1436, doi:10.1016/j.carbpol.2012.07.011.

[38] A. Duconseille, T. Astruc, N. Quintana, F. Meersman, V. Sante-Lhoutellier, Gelatin structure and composition linked to hard capsule dissolution: a review, Food Hydrocoll 43 (2015) 360–376, doi:10.1016/j.foodhyd.2014.06.006.

[39] G.T. Hermanson, Bioconjugate Techniques, Academic Press, London, 2008.

[40] B.T. Hofreiter, B.H. Alexander, I.A. Wolff, Rapid estimation of dialdehyde content of periodate oxystarch through quantitative alkali consumption, Anal. Chem. 27 (1955) 1930–1931, doi:10.1021/ac60108a023.

[41] J. Steck, S. Hassan, Z. Suo, Fracture initiated from corners in brittle soft materials, J. Mech. Phys. Solids. 170 (2023) 105115, doi:10.1016/j.jmps.2022.105115.

[42] T. Igarashi, Mechanics of peeling of rubbery materials. I. Peel strength and energy dissipation, J. Polym. Sci. Polym. Phys. Ed. 13 (1975) 2129–2134, doi:10.1002/pol.1975.180131106.

[43] J. Liu, C. Yang, T. Yin, Z. Wang, S. Qu, Z. Suo, Polyacrylamide hydrogels. II. Elastic dissipater, J. Mech. Phys. Solids. 133 (2019) 103737, doi:10.1016/j.jmps.2019.103737.

[44] Baxter Healthcare Corporation, Full prescribing information for TISSEEL. https://baxterpi.com/pi-pdf/Tisseel_PI.pdf, 2019 (accessed 11 October 2023).